DIAMOND CRYSTALS AND THEIR MINERAL INCLUSIONS FROM THE LYNX KIMBERLITE DYKE COMPLEX, CENTRAL QUEBEC

ADRIAN D. VAN RYTHOVEN[§]

Department of Geology, University of Toronto, Erindale College, Mississauga, Ontario L5L 1C6, Canada

TOM E. McCANDLESS[¶]

Stornoway Diamond Corporation, 116-980 West 1st Street, North Vancouver, British Columbia V7P 3N4, Canada

DANIEL J. SCHULZE

Department of Geology, University of Toronto, Erindale College, Mississauga, Ontario L5L 1C6, Canada

ANTHONY BELLIS

Stornoway Diamond Corporation, 116-980 West 1st Street, North Vancouver, British Columbia V7P 3N4, Canada

LAWRENCE A. TAYLOR AND YANAN LIU

Planetary Geosciences Institute, Department of Earth and Planetary Sciences, University of Tennessee, Knoxville, Tennessee 37996, U.S.A.

ABSTRACT

Lynx is a 522 Ma kimberlite dyke complex located in the Otish Mountains of central Quebec, Canada. Test sampling of the Lynx kimberlite yielded 6598 macrodiamond samples from 528 t of kimberlite. Single crystals strongly dominate the population, with only 14% of the macrodiamond portion consisting of macles and aggregates. Within the single crystals, 41% are dominated by octahedral surface features, and the remaining ones are partially resorbed tetrahexahedroida. Brown is the most common color among the tetrahexahedroida, with only 22% gray to colorless stones comprising the remainder. In contrast, the octahedra are roughly equal in numbers of brown, gray and colorless stones. A subset of twenty stones was selected in the –11 to +3 DTC (0.256 c to 0.67 c) range of circular sieve sizes on the basis of visible inclusions. These have octahedral primary growth-forms and include three macles and three aggregates of octahedra. Most of the samples are significantly resorbed; they range from octahedra with rounded corners and edges to tetrahexahedroida. Shield laminae, serrate laminae, and hillocks are the most common resorption-related surface features. The stones were cut and polished along single planes to expose mineral inclusions for analysis and to allow imaging of internal structure of the diamond relative to the inclusions. Cathodoluminescence imaging revealed deformation lamellae in most of the polished crystals. Some exhibit deformation lamellae truncated by growth or resorption zones or intersections of different crystallographic planes. Oscillatory patterns of planar growth with complex cores are most common. Inclusions, particularly of olivine, typically occur in core and early growth regions of the diamond crystals. Primary inclusions exposed by polishing are magnesian olivine, chromian diopside, chromian pyropic garnet, magnesian orthopyroxene, omphacite, and sulfide. The chromian diopside inclusions yield equilibration conditions in the range of 58–60 kbar and 1250–1280°C that correspond to conditions slightly below a 42 mW/m^2 surface heat-flow geothermal gradient. The most iron-rich olivine inclusion (mg# = 0.916) occurs with the diopside inclusions, suggesting a relatively fertile lherzolitic component of mantle at 180–190 km depth. The garnet data indicate that within the peridotite parentage, both harzburgitic (three G10, 12.4–13.7 wt.% Cr_2O_3, 3.7–4.4 wt.% CaO) and lherzolitic (one G9, 8.9 wt.% Cr_2O_3, 5.8 wt.% CaO) parageneses are present.

Keywords: kimberlite, diamond, inclusion, cathodoluminescence, morphology, deformation, chemistry, Lynx dyke complex, central Quebec.

[§]   *E-mail address*: adrian.vanrythoven@utoronto.ca
[¶]   *Present address*: MCC Geoscience, Inc., North Vancouver, British Columbia V7P 3G6, Canada.

Sommaire

Nous décrivons le complexe de filons kimberlitiques de Lynx, mis en place il y a 522 million d'années dans les montagnes Otish, dans la région centrale de Québec, au Canada. L'échantillonage a produit 6598 macrodiamants à partir de 528 t de kimberlite. Les monocristaux sont prédominants, avec seulement 14% des macrodiamants sous forme de macles et d'agrégats. Parmi les monocristaux, 41% montrent surtout une morphologie octaédrique, et les autres sont des tétrahexaédroïdes partiellement résorbés. La plupart de ces tétrahexaédroïdes sont bruns, et seulement 22% du reste sont gris à incolores. En revanche, la population des octaèdres est faite à parts égales de cristaux bruns, gris et incolores. Un groupe de vingt pierres a été choisi dans l'intervalle de grandeur de tamis circulaires allant de −11 à +3 DTC (0.256 c à 0.67 c) pour une étude des inclusions visibles. Ces pierres sont octaédriques et comprennent trois individus maclés et trois agrégats d'octaèdres. La plupart de ces pierres ont été résorbées de façon importante. On voit des octaèdres avec coins et arêtes arrondis et des tétrahexaédroïdes. La résorption a surtout produit des lamelles en bouclier, des lamelles dentelées et des amoncèlements. Ces pierres ont été coupées et polies afin d'analyser les inclusions minérales et d'illustrer la structure interne du diamant par rapport à celle des inclusions. Les images préparées en cathodoluminescence révèlent des lamelles de déformation dans la plupart des cas. Certains font preuve de lamelles de déformation tronquées par des zones de croissance ou de résorption, ou des intersections de plans cristallographiques. Les cas de croissance planaire oscillatoire sur un noyau complexe sont les plus communs. Les inclusions, surtout de l'olivine, sont surtout développées dans le noyau et les parties précoces des cristaux de diamant. Les inclusions primaires mises en évidence par polissage sont l'olivine magnésienne, le diopside chromifère, le pyrope chromifère, l'orthopyroxène magnésien, l'omphacite et un sulfure. Les inclusions de diopside chromifère indiquent des conditions d'équilibrage dans l'intervalle 58–60 kbar et 1250–1280°C, légèrement en dessous d'un gradient géothermique calculé pour un flux de chaleur de 42 mW/m^2. On trouve l'inclusion d'olivine la plus enrichie en fer (mg# = 0.916) avec les inclusions de diopside, ce qui fait penser qu'il y a un manteau lherzolitique relativement fertile à une profondeur de 180–190 km. Les données sur le grenat indiquent une filiation péridotitique, soit harzburgitique (trois cristaux G10, 12.4–13.7% Cr$_2$O$_3$, 3.7–4.4% CaO), soit lherzolitique (un cristal G9, 8.9% Cr$_2$O$_3$, 5.8% CaO).

(Traduit par la Rédaction)

Mots-clés: kimberlite, diamant, inclusion, cathodoluminescence, morphologie, déformation, composition chimique, complexe de filons Lynx, Québec central.

Introduction

Primary (*i.e.*, protogenetic and syngenetic) mineral inclusions in diamond represent the most pristine samples of mantle material available (*e.g.*, Meyer 1987), owing to the impermeable and unreactive character of diamond. Following the discovery of diamond on the Archean Slave craton in the Canadian Arctic in the early 1990s, diamond exploration has expanded to other Archean cratons in North America. This follows the empirical observation made by Clifford (1966) that diamond deposits typically occur in cratons tectonically stable for the last 1.5 Ga. The largest exposed Archean craton in the world, the ~2.7 Ga Superior craton (Davis 2002), constitutes most of the eastern half of Canada. This craton is host to numerous occurrences of kimberlite and other rocks that have arisen from deep within the lithosphere: Wawa (*e.g.*, Lefebvre *et al.* 2003, 2005, De Stefano *et al.* 2006, Stachel *et al.* 2006), Attawapiskat (*e.g.*, Scully 2000, Webb *et al.* 2004), Kirkland Lake (*e.g.*, Vicker 1997), Temiscamingue (*e.g.*, Heaman *et al.* 2004), and the Foxtrot property in the central Otish Mountains, Quebec (Fig. 1a). Although diamond exploration has been conducted in the Superior craton since the 1950s, no significant discoveries were made until the 1990s to early 2000s.

In contrast to large datasets for mineral inclusions in diamond from other, much smaller cratons such as the Kaapvaal (*e.g.*, Meyer & Boyd 1972, Tsai *et al.*

1979) and the Slave (*e.g.*, Davies *et al.* 2004), previous studies of inclusion suites in diamond from the Superior craton have been very limited. Only studies from suites in Wawa, Ontario (De Stefano *et al.* 2006, Stachel *et al.* 2006) and the nearby Renard, Quebec (Hunt *et al.* 2008), kimberlitic bodies have been published. To address the paucity of data for the Superior craton, we present a study of diamond crystals and their mineral inclusions from the Lynx kimberlite, also in Quebec. We have characterized the morphology of a representative sample of the population of Lynx diamond xenocrysts recovered through bulk sampling operations. A subset of twenty stones was selected for chemical analysis on the basis of visible inclusions. The diamond crystals were polished to expose the inclusions and to characterize growth zoning using cathodoluminescence.

Background Information

The Foxtrot property contains several types of kimberlite bodies (projects) currently under evaluation for diamond potential: the Renard kimberlite diatremes (*e.g.*, Fitzgerald *et al.* 2009), the Hibou kimberlite dyke, and the Lynx kimberlite dyke complex (Fig. 1b). The property is jointly owned by Stornoway Diamond Corp. and SOQUEM. Diamond grade at Lynx is estimated to be 0.47–2.56 c/t (carats per metric tonne), with a diamond value of 56–97 US$/c (United States $ per carat; Stornoway website news release April 28th, 2008).
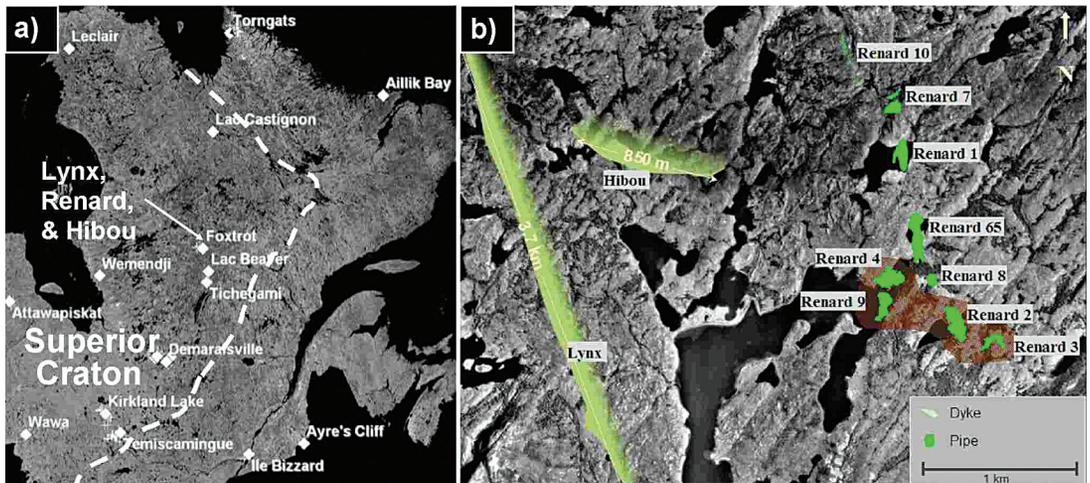
FIG. 1.   a) Satellite photograph of the eastern Superior craton with kimberlitic occurrences indicated. The distance from Attawapiskat to Foxtrot is approximately 780 km. Dashed line: approximate boundary of the Superior Craton. b) Smaller scale photograph of the Foxtrot property, with the Lynx and Hibou kimberlite dykes indicated along with the Renard bodies. Brown-red shading of Renard 2, 3, 4, 8, and 9 bodies indicates deposits included in current mine development. Modified after original map images from Stornoway Diamond Corporation.

FIG. 2.   A representative selection of diamond crystals from Lynx in the +11 DTC sieve category (3.45–4.52 mm). From left to right: grey, brown, light brown, and colorless stones. Note the stone in the far left grey group with brownish stripes.

The Lynx dyke complex in the Otish Mountains region of Quebec (Fig. 1) was discovered in 2003 by Ashton Mining of Canada (now part of Stornoway Diamond Corporation) and its joint-venture partner SOQUEM. It is a series of *en échelon* dykes striking NNW over four kilometers, with a maximum width of 3 m. Although it is only 2 km west of the 630–640 Ma Renard kimberlite cluster (U–Pb perovskite, Birkett *et al*. 2003), Lynx is approximately one hundred million years younger at 522 ± 30 Ma (McCandless *et al*. 2008) based on U–Pb dating of groundmass ilmenite (Noyes *et al*. 2011).

SAMPLES

In 2005, trench sampling of the Lynx dyke recovered 700 macrocrysts of diamond constituting approximately

42 c (carats), from 34 t of hypabyssal kimberlite. In 2007, a larger trenching program recovered 5898 stones (~529 c) from 494 t, including a 22 c brownish octahedron, the largest crystal of diamond found to date in Quebec.

Morphological and color characteristics were documented for all crystals exceeding 0.67 c: 30 and 18 stones in the 3Gr (0.67 to 0.9 c) and 4Gr (0.91 to 1.2 c) size classes, respectively. Representative splits of 50 to 100 stones were taken from the +3 to +11 (*e.g.*, Fig. 2) DTC (Diamond Trading Company classification) circular sieve categories (1.47 to 3.45 mm, or ~0.03 to 0.67 c/stone). Stones for the inclusion study were taken from the parcel of 700 recovered in 2005. Inclusion abundances for the larger size-population were not determined. The stones selected range in size from 0.03 to 0.45 c and are roughly representative of

the larger 2007 sample population. Sixteen contain primary mineral inclusions (Table 1). Inclusions of epigenetic (late alteration) minerals include serpentine, Ca–Mg carbonates, phlogopite, Mg–Fe±Al silicates, and various Fe–Ti oxides. These minerals were determined to be epigenetic on the basis of their exposure reaching the surface of the diamond prior to cutting (*e.g.,* along cracks) and by their very fine-grained, polycrystalline nature.

ANALYTICAL METHODS

The diamond crystals were cut and polished so as to expose as many inclusions as possible. No attention was given to crystallographic orientation, although most were cut parallel or subparallel to {110}. Planes created by cutting and polishing were imaged in reflected light and with back-scattered electron (BSE) and secondary electron methods using a JEOL scanning electron microscope. At this stage, the identities of mineral inclusions were qualitatively characterized using energy-dispersive X-ray spectrometry.

The internal structures of the cut stones were imaged using cathodoluminescence (CL) with a Vickers Instruments Nanolab LE2100 instrument at the Royal Ontario Museum. The electron gun potential used was 15 kV at 0.272 nA, with a working distance of 30.4 mm. Several crystals were imaged using CL under similar conditions

TABLE 1. THE SIXTEEN CRYSTALS OF DIAMOND FROM THE LYNX KIMBERLITE DYKE
WITH EXPOSED PRIMARY INCLUSIONS

Sample	Incl.	Parag.	Color	Morphology	Surface features	CL zoning
Lynx1	ol	P	light brown	mac	herringbone mirror plane	simple layered growth, deformation laminae
Lynx3	ol	P	light brown	oct frag	some corrosion sculpture	both complex irregular and layered growth
Lynx4	opx	P	light brown	oct	shield laminae, ribbing, (-) trigons	fairly complex high-response core, low-response outer simple layered growth, deformation laminae
Lynx6	grt, ol	P(h)	red-brown	slightly dist res oct	ruts	complex layered growth
Lynx7	ol, opx	P	light brown	slightly res oct	shield laminae	very complex irregular core with outer layered growth
Lynx8	4x ol	P	light brown	oct agg	ruts, frosting, pitting	very complex irregular and layered growth, deformation laminae
Lynx12	sul	P	grey	3 intergrown oct	shield laminae, ribbing	complex partly low-response core with outer oscillatory growth, deformation laminae
Lynx15	3x ol	P	light brown	res dist oct	hillocks	complex euhedral core with homogeneous outer zone, deformation laminae
Lynx16	2x grt	P(h)	light brown	2 res intergrown oct	shield laminae, ribbing	pseudohemimorphic high-response core with layers, simple outer zone, deformation laminae
Lynx17	2x ol	P	light brown	res oct-thh	frosting, hillocks	complex core, layered outer growth, deformation laminae
Lynx18	ol	P	light red	dist res oct	terraces, hillocks	simple layered growth, some deformation laminae
Lynx19	ol	P	light brown	res thh agg	terraces, hillocks	very complex high-response core, oscillatory outer zone, deformation laminae
Lynx20	grt, ol	P(l)	red-brown	oct	ruts, (-) trigons	large homogeneous inner zone, layered outer zone
Lynx21	omp	E	color-less	thh	some frosting	complex but layered growth, possible twin plane
Lynx24	7x cpx ol	P(l)	red-brown	res thh agg	terraces, hillocks	patchy irregular growth with low-response infilling textures
Lynx27	2x ol	P	light brown	thh	some frosting	very complex patchy core with layered outer zones

Symbols: ol: olivine, opx: orthopyroxene (enstatite), grt: chromian pyropic garnet, sul: sulfide, omp: omphacite, cpx: chromian diopside, mac: macle, oct: octahedron, frag: fragmented, dist: distorted or deformed, res: resorbed, agg: aggregate, thh: tetrahexahedroid, (–): negative. Paragenesis; E: eclogitic, P: peridotitic, l: lherzolitic, h: harzburgitic.

at the Geological Survey of Canada, Ottawa, and at the Department of Geology, University of Toronto (20 kV at 1–2 nA).

The primary mineral inclusions identified using SEM methods were quantitatively analyzed with a Cameca SX–50 electron microprobe using a 1 μm beam and wavelength-dispersion spectrometry methods of detection as at the Duncan Derry Laboratory, University of Toronto. Accelerating voltages and beam currents used were 20 kV and 45 nA for sulfide analyses, 20 kV and 30 nA for olivine, and 15 kV and 30 nA for orthopyroxene, clinopyroxene, and pyrope inclusions. Higher potential and current were used for the olivine and sulfide inclusions to obtain higher-quality analyses for nickel, and because of the higher concentrations of mobile elements (*i.e.,* potassium, sodium) in garnet and pyroxene. We provide detection limits and count times in Table 2.

CHARACTERISTICS OF THE DIAMOND CRYSTALS

Color and morphology

Color and morphological features were determined for single, unbroken stones. Many of the crystals have surface features that are interpreted to be due to resorption, which has modified octahedral to tetrahexa-hedroidal surfaces. Shield and serrate laminae (after Robinson *et al*. 1989) on partially resorbed {111} faces are the most common feature on the surfaces of the octahedra. Negative trigons are present on two of the sixteen octahedra with exposed primary inclusions. Fine to coarse hillocks are the dominant feature on tetrahexahedroidal surfaces. Fifteen percent of the

diamond crystals larger than 0.66 c, and 43% of stones below 0.66 c, display uneven resorption (pseudohemi-morphism; *cf.* Robinson *et al.* 1989). Post-emplacement corrosion-induced sculpture and frosting are surface features developed on both octahedral and tetrahexahedroidal surfaces on several of the diamond crystals. It is most evident on larger stones, but was not sought in smaller ones. Therefore, a statistical value of corrosion sculpture for the population is not possible.

In the size ranges assessed (and excluding irregular cases), 13% of the stones are macle twins, 1% are aggregates, and 86% are single crystals (Fig. 3a). Of the 4549 single crystals, 59% are tetrahexahedroidal and 41% are relatively unresorbed octahedra (Fig. 3b). The tetrahexahedroida are mostly of light brown to brown color (78%), whereas the octahedra are almost equal in proportions of brown, colorless, and grey crystals (Figs. 3c, d). Some stones exhibit "patchy" or "striped" brownish coloration (*e.g.,* Fig. 2, far left). Twin and aggregate stones are dominantly octahedral, being relatively unresorbed.

In the larger size-ranges, macles and aggregates constitute 33% of the diamond population (Fig. 4a). Resorption is most evident in the intermediate size (–11 to +9 DTC) category (Fig. 4b). Light brown to brown stones are most common in the –9 to +7 and –11 to +9 DTC sieve size-categories. The highest proportions of colorless and grey stones are in the smaller (–5 to +3: 44%; –7 to +5: 50%) categories, with an intermediate proportion in the larger categories (22–33%, Fig. 4c).

In the subset of twenty inclusion-bearing diamond crystals, light brown to brown is the dominant body color, and octahedral (and tetrahexahedroidal variants due to resorption) surfaces dominate. Only one colorless

TABLE 2. DETECTION LIMITS AND COUNT TIMES IN MINERAL ANALYSES

	Detection limits[§]									
Mineral	Na$_2$O	MgO	Al$_2$O$_3$	SiO$_2$	K$_2$O	CaO	TiO$_2$	Cr$_2$O$_3$	MnO	FeO	NiO
olivine	–	0.006	n.a.	0.007	–	0.007	–	0.013	0.025	0.02	0.018
pyroxene	0.016	0.015	0.013	0.015	0.011	0.021	0.021	0.033	0.019	0.027	0.056
garnet	0.014	0.018	0.019	0.019	–	0.019	0.02	0.028	0.034	0.031	–

Mineral	Fe	Cu	Ni	Co	S
sulfide	0.022	0.048	0.014	0.025	0.019

	Count times[¶]									
Mineral	Na$_2$O	MgO	Al$_2$O$_3$	SiO$_2$	K$_2$O	CaO	TiO$_2$	Cr$_2$O$_3$	MnO	FeO	NiO
olivine	–	80	–	64	–	120	–	120	48	80	120
pyroxene	44	32	32	31	96	60	40	40	100	60	20
garnet	96	20	20	20	–	40	60	60	40	60	–

Mineral	Fe	Cu	Ni	Co	S
sulfide	40	40	80	80	40

The analyses were made with a Cameca SX-50 electron microprobe. The detection limits are expressed in weight %. The count times are expressed in seconds, and include on- and off-peak times.
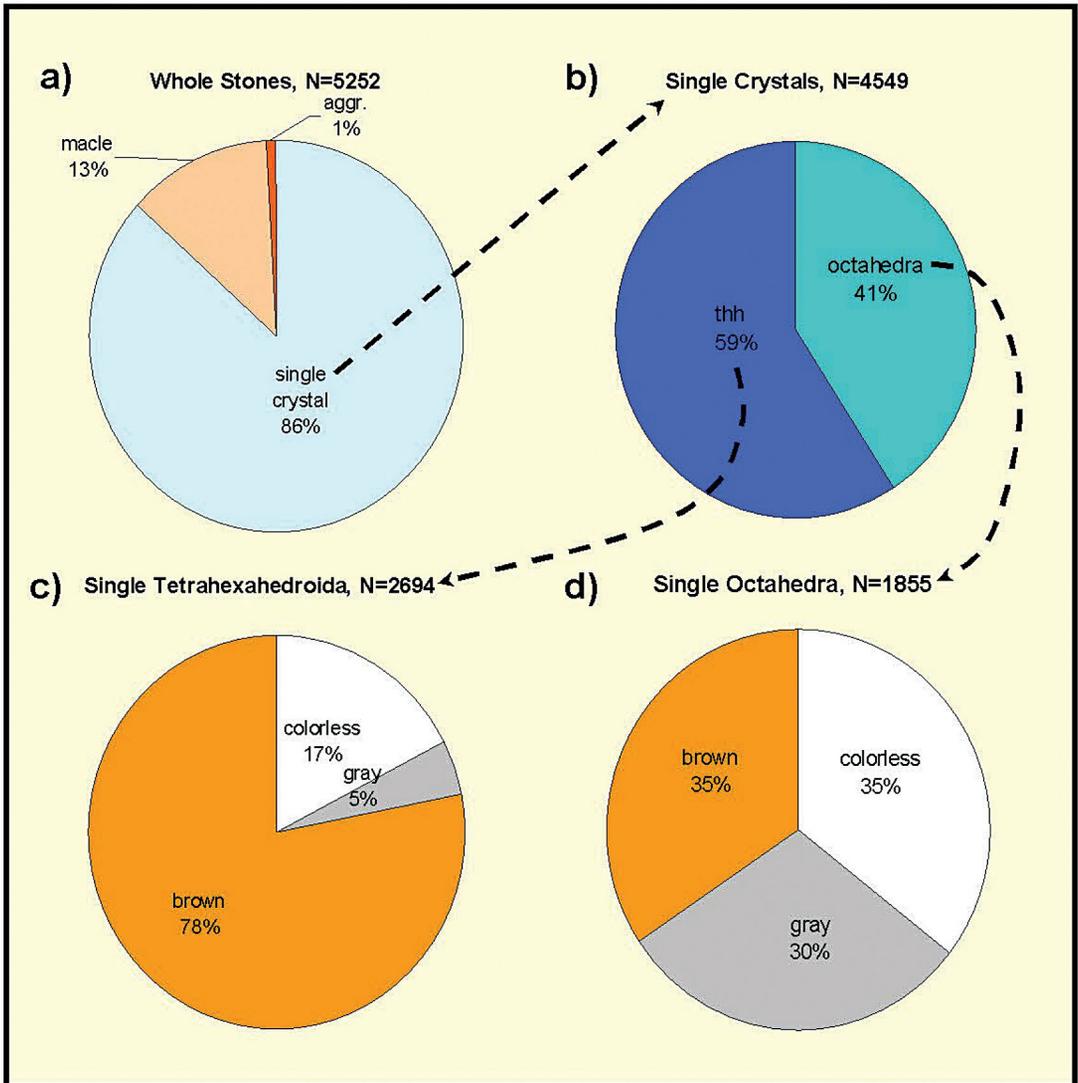
Fig. 3.   Physical characteristics of whole diamond crystals from Lynx (*i.e.*, excluding 1348 heavily fragmented diamond crystals). a) Single stones *versus* twinned and aggregate stones. b) Proportion of tetrahexahedroidal (resorbed) *versus* octahedral (unresorbed) stones. c) Color distribution of tetrahexahedroidal stones. d) Color distribution of octahedral stones.

stone (Lynx21), a tetrahexahedroid, was found to have inclusions suitable for analysis.

Internal structure

The twenty diamond crystals imaged using CL (Fig. 5) have a variety of growth patterns, from simple (*e.g.,* stone number Lynx20) to complex (*e.g.,* Lynx8). For thirteen stones, the surface of the diamond exposed approximately conforms to the {110} orientation

(*e.g.,* Lynx4, Lynx15, Lynx16, Lynx20). However, the remaining seven stones (*e.g.,* Lynx8) were cut at orientations oblique to the {111} plane (*e.g.,* near {112} or {113}). This was done to expose the maximum number of mineral inclusions possible, but makes interpretation of the CL images more difficult. Many (four minimum) of the stones have deformation lamellae, indicated by high-contrast parallel bands cross-cutting the diamond, but unrelated to sample topography, ruling out scratches from polishing (*e.g.,* Lynx8, Lynx15). A common

growth-induced pattern of the crystals is characterized by a complex core with a simpler (generally layered) rim zone seen in seven stones (*e.g.,* Lynx4, Lynx15, Lynx16). Most of the mineral inclusions appear to be located in the core zones of diamond crystals that share this pattern. Five stones appear to have complex, irregular growth-histories (*e.g.,* Lynx8). Eight stones have simpler, oscillatory growth throughout (*e.g.,* Lynx20).

INCLUSIONS IN THE LYNX DIAMOND CRYSTALS

Inclusion compositions

Primary mineral inclusions were exposed in sixteen crystals of diamond. Forsteritic olivine, chromian diopside, chromian pyrope, enstatite, omphacite, and Fe–Ni–Cu sulfide occur in the Lynx stones in order of decreasing abundance (Table 1). Results of the electron-microprobe analyses for these inclusions are presented in Table 3.

Olivine

Seventeen grains of olivine occur in ten crystals. They range in mg# [molar Mg/(Mg + Fe)] from 0.923 to 0.933 (Table 3), with two clusters averaging around 0.924 and 0.932 (Fig. 6). One outlier with mg# = 0.916 occurs in the diamond with seven diopside inclusions.

Pyroxene

Diopside is present as seven inclusions in one sample (Lynx24). These have nearly identical compositions: ~2.3 wt.% Cr_2O_3 and mg# ≈ 0.92 (Table 3). Two diamond crystals with single enstatite inclusions (mg# ≈ 0.94, Al_2O_3 ≈ 0.32) also occur. One grain of omphacite with ~4.1 wt.% Na_2O and ~7.1 wt.% Al_2O_3 is the only inclusion with an eclogitic affinity present in the suite.

Garnet

Four inclusions of pyrope occur in three diamond crystals. One sample (Lynx20) contains a pyrope crystal with a more calcium-rich (~5.8 wt.% CaO) and Cr-poor (~8.9 wt.% Cr_2O_3) composition than the other three inclusions of pyrope in the sample set (3.7–4.4 wt.% CaO, 12.4–13.7 wt.% Cr_2O_3). The Lynx20 pyrope is of lherzolitic paragenesis, and the other three are harzburgitic (Fig. 7). The two crystals of pyrope in one stone (Lynx16) have very similar compositions (Table 3).

Sulfide

One sulfide inclusion was found in diamond Lynx12. It has a high Ni content, in the range 13.6–20.2 wt.%, indicating a peridotitic paragenesis (Yefimova *et al.* 1983, Bulanova *et al.* 1996). Five point-analyses yielded five different compositions, indicating sample

heterogeneity (Table 3). This was confirmed by X-ray element mapping, which shows spatial variation in concentrations of the major metals nickel, iron, and copper, with no sharp compositional boundaries (Figs. 8a, b). This is not evident using BSE imaging (Fig. 8c).
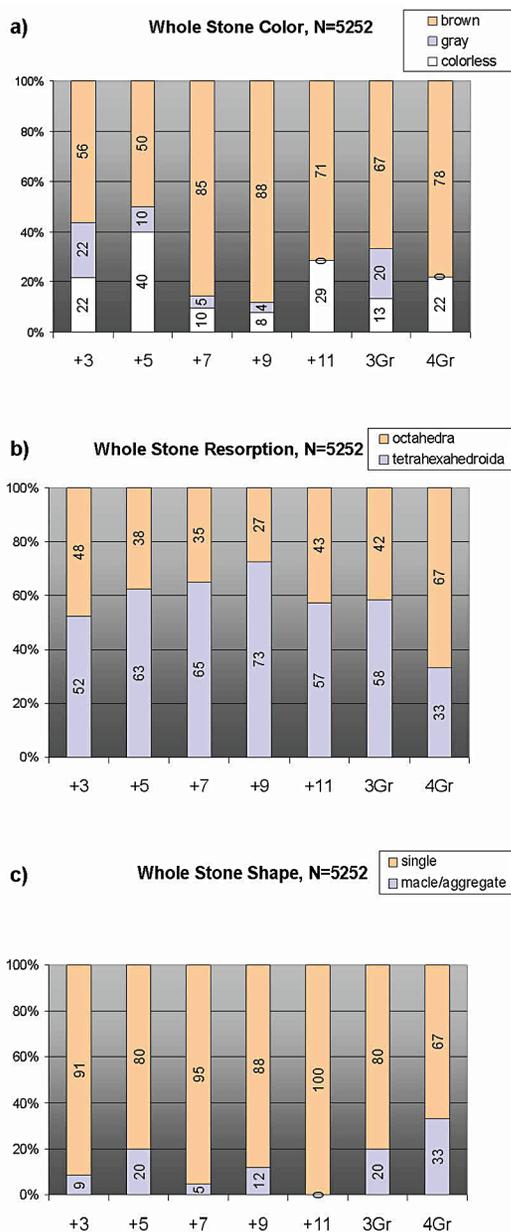
FIG. 4. Physical characteristics of whole stones from Lynx by size (sieve) class: a) color, b) morphology (degree of resorption), c) single *versus* polycrystalline stones.
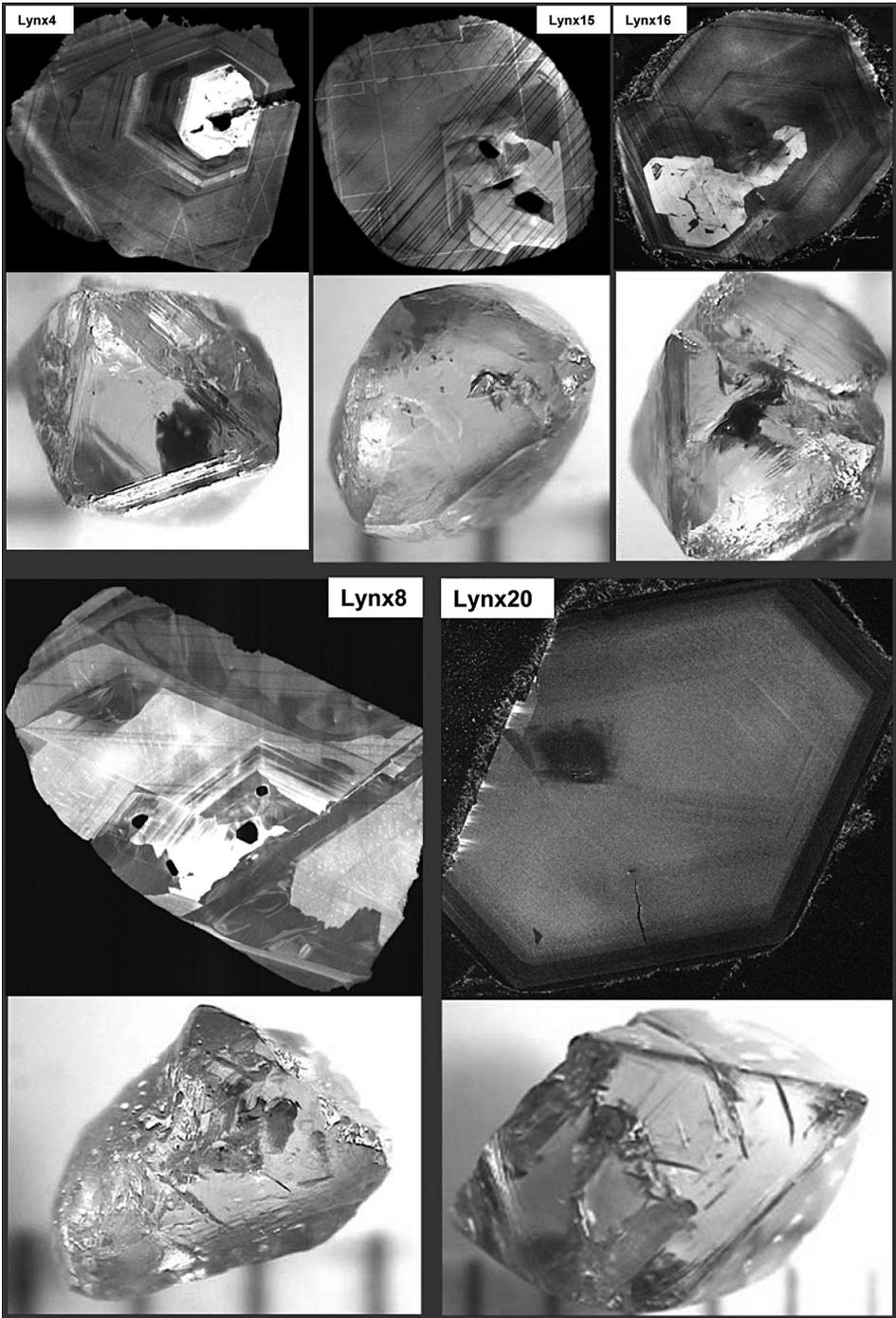
Fig. 5.   Photomicrographs of diamond crystals from Lynx with millimeter scale bars (bottom) and CL images of the stones after cutting and polishing (top). Samples names are as labeled. Note: the bright orthogonal lines on CL images of Lynx4 and Lynx15 are due to electron-beam damage during the electron-microprobe analysis and are not sample-related.
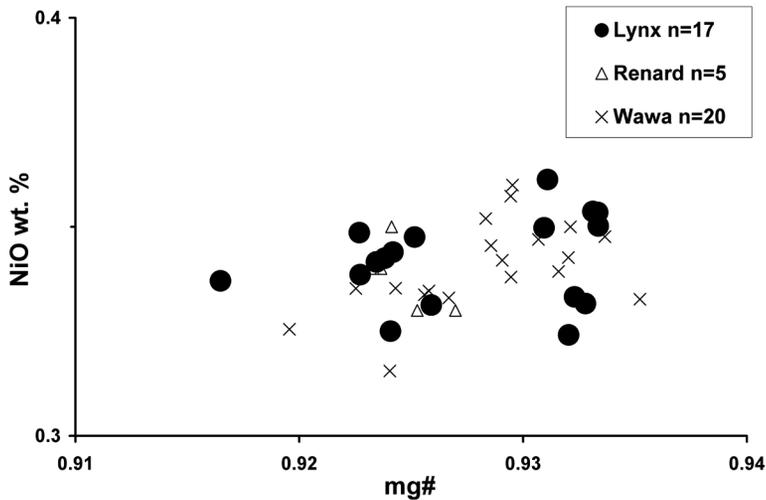
FIG. 6.   NiO (wt.%) *versus* mg# plot for olivine inclusions in diamond from Lynx (this study), Wawa (De Stefano *et al.* 2006, Stachel *et al.* 2006), and Renard (Hunt *et al.* 2008).
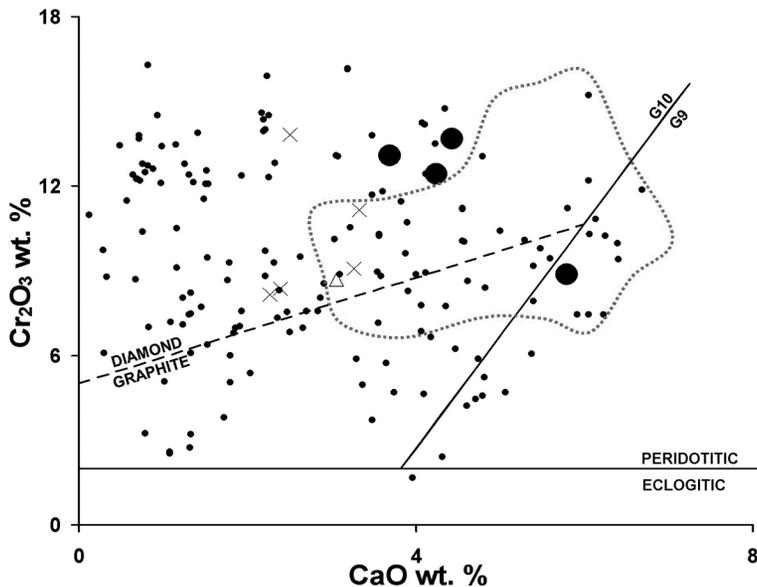
FIG. 7.   Plot of weight % CaO *versus* Cr_2O_3 for garnet inclusions in diamond from Lynx (large dots, n = 4, this study), Wawa (crosses, n = 5, Stachel *et al.* 2006) and Renard (triangle, n = 1, Hunt *et al.* 2008). Small dots: peridotitic garnet inclusions in diamond from the southern African (n = 109, Viljoen *et al.* 1999, Stachel *et al.* 2004) and Siberian (n = 52, Sobolev 1977, Sobolev *et al.* 1978, 1984, 1999, 2004) cratonic regions. Dotted line: compositional field for pyrope in diamond from the Slave craton (n = 27, Davies *et al.* 1999, Pokhilenko *et al.* 2004, Tappert *et al.* 2005, Donnelly *et al.* 2007). Graphite–diamond constraint (dashed line, assuming 38 mW/m^2 geotherm) from Grütter *et al.* (2006). The G10–G9 fields of affinity of eclogitic garnet inclusions are taken from Gurney (1984).
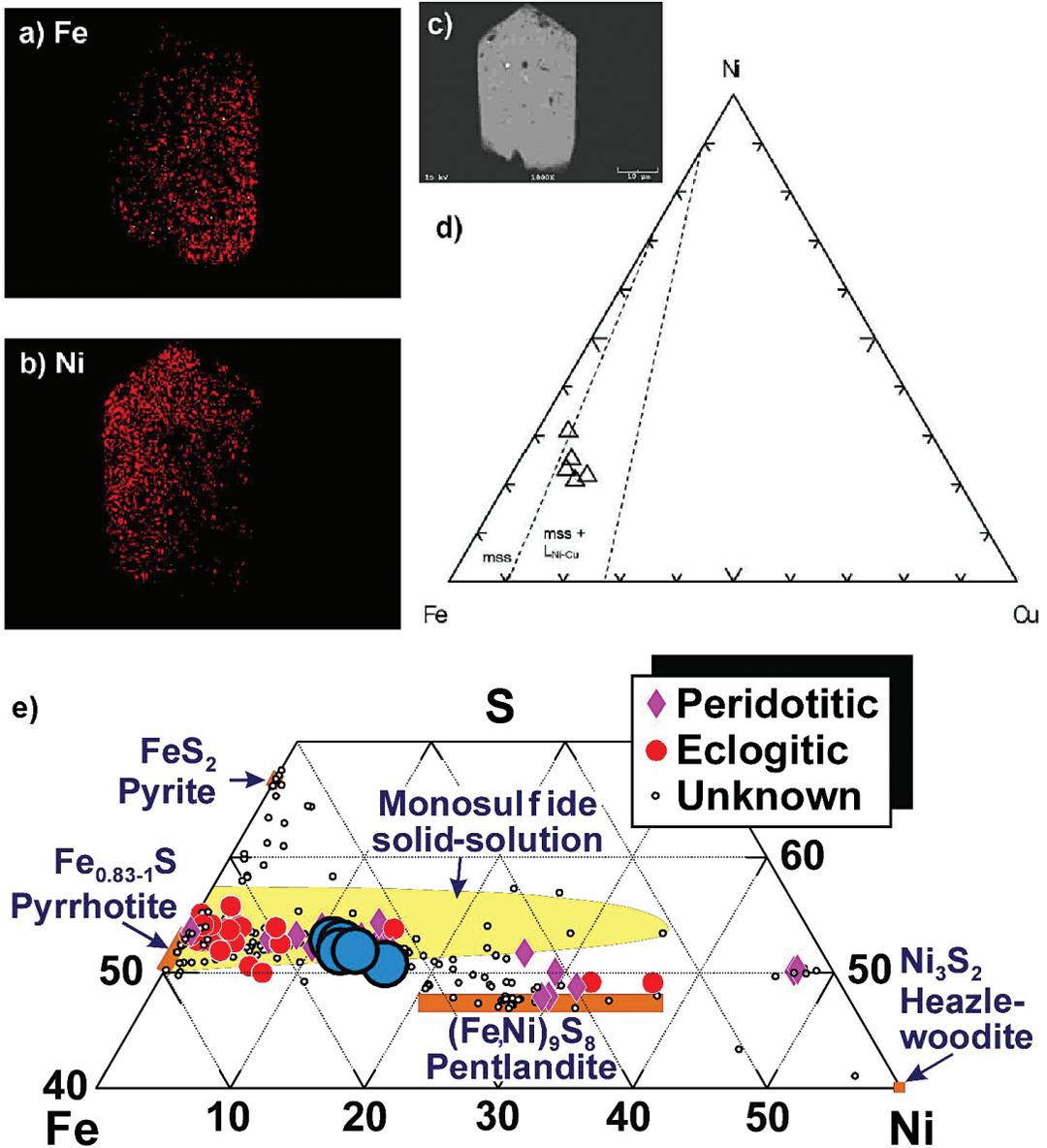
FIG. 8.   a) Fe X-ray map of sulfide inclusion Lynx-12-1. b) Ni X-ray map of sulfide inclusion Lynx-12-1. c) BSE image of sulfide inclusion Lynx-12-1. d) Phase relations in the Fe–Ni–Cu (atomic proportions) sulfide system at 1000°C and 1 atm, from Craig & Kullerud (1969). Symbols: *mss*: monosulfide solid-solution, *mss* + L_{Ni-Cu}: monosulfide solid-solution mineral in equilibrium with a Ni–Cu-rich sulfide liquid. Point analyses for sulfide inclusion Lynx-12-1 are shown (triangles). e) Phase-relation diagram for the Fe–S–Cu (atomic proportions) ternary system. Compositions of pyrrhotite, pyrite, pentlandite, and heazlewoodite shown as orange fields. Experimentally determined field for monosulfide solid-solution at 1000°C and 1 atm is shown in yellow. Point analyses for sulfide inclusion Lynx-12-1 are shown (large blue circles). World data for sulfide inclusions of peridotitic (orange dots), eclogitic (pink diamonds), and unknown parageneses (small black circles) are shown. Plot modified after Stachel & Harris (2008).

In terms of an Fe–Cu–Ni diagram, the compositions all correspond to monosulfide solid-solution (*mss*) in equilibrium with metal sulfide liquid (L) field at 1000°C after Craig & Kullerud (1969) (Fig. 8d). In an Fe–Ni–S ternary diagram, there is a clear trend toward exsolution of pentlandite from *mss* (Fig. 8e). It is likely that this inclusion was originally *mss*, but upon cooling, underwent exsolution of pentlandite and copper-rich pyrrhotite (± pyrite and chalcopyrite) to create the complex mixture (*e.g.,* Taylor & Liu 2009).

Geothermobarometry

The geothermobarometer of Nimis & Taylor (2000) based on chromium and calcium in diopside was applied to the seven inclusions of diopside in Lynx24 and resulted in an average temperature and pressure of equilibration of 1270°C and 59 kbar (185 km depth). This corresponds to equilibrium conditions slightly below the 42 mW/m^2 (Fig. 9) surface heat-flow and conductive geothermal gradient of Pollack

TABLE 3. RESULTS OF ELECTRON-MICROPROBE ANALYSES OF PRIMARY MINERALS EXPOSED
BY CUTTING AND POLISHING THE LYNX STONES

	Lynx 6-1 grt	Lynx 20-1 grt	Lynx 16-1 grt	Lynx 16-2 grt	Lynx 24-1 cpx	Lynx 24-2 cpx	Lynx 24-3 cpx	Lynx 24-4 cpx	Lynx 24-5 cpx	Lynx 24-6 cpx	Lynx 24-7 cpx	Lynx 24-8 ol	Lynx 21-1 omp	Lynx 4-1 opx	Lynx 7-2 ol	Lynx 7-3 opx
SiO$_2$ wt.%	41.70	42.58	40.61	41.04	55.36	55.35	55.58	55.34	55.40	55.34	55.54	41.60	55.20	58.58	41.38	58.30
TiO$_2$	0.11	0.04	0.01	0.05	0.02	0.04	0.04	0.04	0.03	0.06	0.02	---	0.39	0.00	---	0.00
Al$_2$O$_3$	13.76	15.09	13.17	12.78	1.68	1.68	1.71	1.73	1.70	1.76	1.74	---	7.10	0.31	---	0.32
Cr$_2$O$_3$	12.43	8.87	13.67	13.07	2.23	2.26	2.32	2.33	2.24	2.32	2.29	0.06	0.25	0.29	0.10	0.32
FeO(t)	5.58	7.43	6.21	6.37	2.87	2.88	2.84	2.83	2.86	2.78	2.82	8.11	5.79	4.18	7.39	4.29
MnO	0.24	0.33	0.34	0.32	0.12	0.13	0.12	0.11	0.12	0.11	0.10	0.13	0.08	0.12	0.13	0.12
NiO	---	---	---	---	0.08	0.07	0.05	0.10	0.04	0.07	0.09	0.34	0.05	0.15	0.34	0.10
MgO	21.87	20.58	20.21	20.89	18.41	18.44	18.26	18.25	18.46	18.28	18.34	49.91	10.98	36.56	50.25	36.15
CaO	4.24	5.79	4.44	3.69	16.71	16.70	16.84	16.88	16.66	16.66	16.72	0.04	15.86	0.30	0.03	0.52
Na$_2$O	0.01	0.03	0.01	0.00	1.96	1.95	2.05	2.03	1.94	2.02	2.07	---	4.08	0.01	---	0.03
K$_2$O	---	---	---	---	0.04	0.04	0.03	0.03	0.03	0.02	0.03	---	0.01	0.01	---	0.01
Total	99.93	100.74	98.67	98.20	99.50	99.54	99.84	99.68	99.48	99.42	99.78	100.18	99.78	100.51	99.62	100.13
mg#	0.88	0.83	0.85	0.85	0.92	0.92	0.92	0.92	0.92	0.92	0.92	0.92	0.77	0.94	0.92	0.94

	Lynx 15-1 ol	Lynx 15-2 ol	Lynx 15-3 ol	Lynx 18-1 ol	Lynx 8-1 ol	Lynx 8-2 ol	Lynx 8-3 ol	Lynx 8-4 ol	Lynx 1-1 ol	Lynx 17-1 ol	Lynx 17-2 ol	Lynx 19-1 ol	Lynx 27-1 ol	Lynx 27-2 ol	Lynx 3-1 ol
SiO$_2$ wt.%	41.45	41.45	41.30	41.47	41.71	41.75	41.58	41.64	41.82	41.31	41.38	41.17	42.00	41.76	41.69
TiO$_2$	---	---	---	---	---	---	---	---	---	---	---	---	---	---	---
Al$_2$O$_3$	---	---	---	---	---	---	---	---	---	---	---	---	---	---	---
Cr$_2$O$_3$	0.05	0.05	0.05	0.09	0.10	0.11	0.08	0.09	0.05	0.05	0.04	0.04	0.05	0.05	0.05
FeO(t)	6.64	6.68	6.71	6.81	6.61	6.62	6.62	6.63	7.61	7.41	7.33	7.31	7.37	7.57	7.28
MnO	0.10	0.09	0.10	0.10	0.08	0.09	0.09	0.09	0.13	0.12	0.12	0.12	0.13	0.12	0.12
NiO	0.33	0.33	0.32	0.35	0.35	0.36	0.35	0.35	0.35	0.34	0.34	0.33	0.35	0.34	0.33
MgO	51.67	51.58	51.62	51.48	51.93	50.18	51.96	51.87	50.95	50.13	50.11	49.92	51.14	50.69	51.06
CaO	0.02	0.02	0.02	0.03	0.02	0.02	0.02	0.02	0.02	0.03	0.02	0.02	0.03	0.03	0.03
Na$_2$O	---	---	---	---	---	---	---	---	---	---	---	---	---	---	---
K$_2$O	---	---	---	---	---	---	---	---	---	---	---	---	---	---	---
Total	100.26	100.19	100.12	100.32	100.80	99.13	100.71	100.69	100.94	99.39	99.34	98.91	101.07	100.55	100.56
mg#	0.93	0.93	0.93	0.93	0.93	0.93	0.93	0.93	0.92	0.92	0.92	0.92	0.93	0.92	0.93

Lynx12-1 (sulfide)

Fe	42.12	39.74	41.03	42.69	41.57
Cu	8.33	3.92	9.59	6.52	6.41
Ni	13.59	20.18	14.44	15.14	16.62
Co	0.08	0.30	0.15	0.11	0.16
S	35.31	34.82	34.77	35.20	35.49
Total	99.43	98.96	99.98	99.64	100.24

All iron is stated as ferrous (FeO$_t$). Results are averaged, with the exception of the sulfide data (Lynx12), where individual analyses cover the range of compositions present in the heterogeneous sulfide inclusion. Symbols of the minerals are as in Table 1.
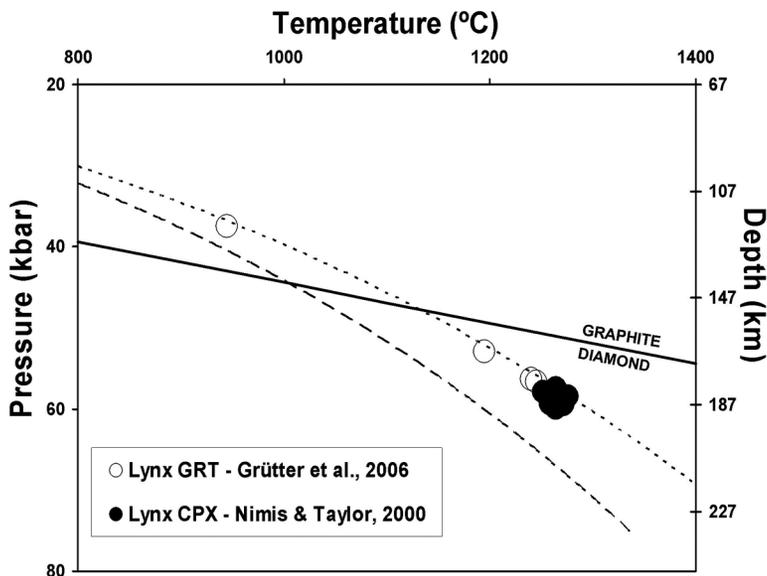
FIG. 9.   Equilibration pressure *versus* temperature plot for clinopyroxene and garnet inclusions in diamond from Lynx. Geothermal gradients with equivalent surface heat-flows of 42 mW/m² (dotted line) and 40 mW/m² (dashed line) are taken from Pollack & Chapman (1977). Diamond–graphite phase boundary is taken from Kennedy & Kennedy (1976). Minimum pressures of equilibration for pyrope inclusions in diamond from Lynx are also projected onto an approximated 41.5 mW/m² geotherm.

& Chapman (1977). Application of the chromium in pyrope geobarometer of Grütter *et al.* (2006) to the four pyrope inclusions from Lynx yields equilibration pressures ranging from 38 to 57 kbar (120–178 km depth). The pyrope inclusion indicative of a lherzolitic paragenesis (Lynx20-1) yields the lowest pressure. As coexisting magnesiochromite inclusions are not present (and magnesiochromite is generally absent as an inclusion phase at Lynx), equilibrium with spinel cannot be assumed and the pressures based on chromium in pyrope clearly represent only minimum values (Grütter *et al.* 2006).

DISCUSSION

Size distribution of diamond crystals

Most regular (*i.e.*, not fragmented) stones from Lynx are single crystals, with macles and aggregates somewhat more common in the coarser sizes. The weaker character of the polycrystalline stones (including macles) may have caused a tendency to break during the recovery process and could explain the lower number of smaller examples.

Brown crystals of diamond form the overwhelming majority of stones from Lynx. This is particularly evident in the +7 to 4Gr size classes. Most tetrahexahedroida are brown in color and dominate all size classes with the exception of 4Gr. There may be a causal relation between resorption and plastic deformation that is partly responsible for red-brown coloration of diamond (*e.g.*, Fisher 2009, and references therein).

A significant portion (43% of stones <0.67 c, 15% of stones ≥0.67 c) of the diamond crystals are pseudo-hemimorphic, suggesting that for these samples, most of the resorption occurred while the diamond was only partially enclosed in the parent rock (peridotite or eclogite).

The high proportions of octahedral to tetrahexahedroidal and brown to colorless diamond crystals from Lynx contrast starkly with those from the neighbouring Renard occurrence, which apparently sampled a different population. Compared to Lynx, typical diamond crystals from Renard are colorless tetrahexahedroida. The proportion of octahedra (30% of stones <0.67 c, 37% of stones ≥0.67 c, see Fig. 4) at Lynx is roughly double that of Renard for similar size-ranges. Furthermore, twin and aggregate stones from Lynx are mostly octahedra, whereas twin and aggregate stones from Renard are mostly tetrahexahedroida (Hunt *et al.* 2008).

Growth history of the diamond crystals

The CL images of the diamond crystals typically have an inclusion-bearing complex core with simpler to homogeneous intermediate and outer zones. This finding suggests for these stones an early history of irregular growth associated with incorporation of mineral inclusions, followed by periodic or steady growth. Deformation laminae typically cross-cut all zones (*e.g.,* Fig. 5: Lynx15), indicating post-growth plastic deformation. However, one sample (Fig. 5: Lynx8) has laminae that are truncated by a fairly straight plane. This plane can either reflect diamond resorption followed by renewed (post-deformational) growth, or a change in crystallographic orientation so that the {111} slip planes would stop at the boundary. Crystal Lynx16 is of particular interest as it has a core with high CL response and includes two G10 pyrope inclusions (Fig. 7, Table 3). This core exhibits both euhedral and irregular boundaries (Fig. 5: Lynx16), possibly reflecting an intermittent stage of resorption before renewed growth.

Parageneses of the inclusions

There are at least four paragenetic groups represented in this small suite of inclusions in diamond crystals from Lynx. A lherzolitic paragenesis is represented by two stones, Lynx20 with a G9 pyrope inclusion and Lynx24 containing seven crystals of chromian diopside and one of low-mg# olivine. A harzburgitic paragenesis is evident for stones containing either subcalcic garnet or high-mg# olivine inclusions. Although garnet inclusion Lynx20-1 plots within the G9 (lherzolitic) field (Fig. 7), it is classified as harzburgitic (along with the other three garnet inclusions in this study) according to the scheme given by Schulze (2003). The third group is eclogitic (the omphacite grain in Lynx21). The fourth "paragenetic group" includes all peridotitic inclusions that cannot be assigned to either the lherzolitic or the harzburgitic suite (sulfide, enstatite, olivine with mg#≈0.92). Thus the diamond population at Lynx appears to be overwhelmingly of P type, although sixteen crystals of diamond is a small set of samples and may not be representative. It is curious that the only E-type mineral occurs in the only truly colorless diamond in the set. All of the P-type crystals have a light brown to brown color. A possible link is that eclogite is more resistant to deformation than peridotite because of the absence of structurally weak olivine, although this suggestion employs significant conjecture.

Comparison of Lynx diamond inclusions with other Superior and worldwide localities

Relative to other cratons, data from inclusions in diamond crystals from the Superior craton are sparse (*e.g.,* Figs. 6, 7). Diamond-inclusion data have been published for only two other localities in the Superior craton, Wawa (De Stefano *et al.* 2006, Stachel *et al.* 2006) and Renard (Hunt *et al.* 2008).

On average, P-type pyrope inclusions from the Superior craton have compositions somewhat more depleted (*i.e.,* extending to lower calcium values, which indicate a higher degree of partial melting) than pyrope inclusions from the only other Canadian craton with diamond-inclusion data, the Slave. They are not as depleted in calcium, however, as are many examples of pyrope inclusions from the Siberian and the southern African cratons (Fig. 7). Though only a single inclusion of pyrope has been reported from Renard, it too belongs to a harzburgitic paragenesis, but with much lower chromium and slightly lower calcium than the three Lynx harzburgitic inclusions (Hunt *et al.* 2008). More pyrope inclusions have been reported at Wawa and have compositions even lower in calcium (Fig. 7). Whereas four of the five reported inclusions of garnet in diamond from Wawa have a significant majorite component (Stachel *et al.* 2006), only pyrope Lynx20-1 could be considered to have a small component of majorite (approximately 0.038 *apfu* Si at the octahedral site, based on [O] = 12 *apfu*).

Olivine inclusions from Lynx have compositions very similar to those from Wawa and Renard (Fig. 6). The olivine inclusions at Lynx are essentially identical to those from Wawa, but appear to plot into three groups (see Results section). The Renard olivine inclusions plot in the intermediate mg# field.

The enstatite inclusions in crystal of diamond from Lynx are very similar to those from Wawa (Stachel *et al.* 2006). The diopside found in Lynx24 is higher in chromium and lower in aluminum than that from Wawa (Stachel *et al.* 2006), but is within the ranges of inclusions in diamond reported from the Siberian and southern African cratons (Sobolev 1977, Tsai *et al.* 1979, Gurney *et al.* 1984, 1985, Wilding *et al.* 1991, Viljoen *et al.* 1999, Sobolev *et al.* 2004). The diopside inclusions in the Lynx suite are richer in chromium (~2.3 wt.% Cr_2O_3) relative to most Slave craton inclusions (0.89–2.3 wt.% Cr_2O_3; Promprated *et al.* 2004, Tappert *et al.* 2005, Donnelly *et al.* 2007, Van Rythoven & Schulze 2009).

Magnesiochromite was not identified in the suite of inclusions. This is unusual for a P-type suite, as magnesiochromite is common in diamond of peridotitic affinity at many localities (*e.g.,* Stachel *et al.* 2003, and references therein). Unlike in the Renard stones, no coesite was found as an inclusion in diamond from Lynx (Hunt *et al.* 2008).

The choice of geothermal gradient corresponding to a surface heat-flow of ~41–42 mW/m² is speculative, as it is essentially based on one point, the average P–T conditions of equilibration for the chromian diopside inclusions in Lynx24. Based on this point, the Lynx kimberlite sampled material as deep as approximately 40 km into the stability field of diamond (Fig. 9). No other data on diopside inclusions in diamond from

the Superior craton (excluding one from Wawa that is unsuitable for use with the Nimis & Taylor geothermobarometer, as its Ca–Cr–Tschermak activity is too low) have been reported.

The geothermal gradient is only slightly cooler than that determined by chromian diopside geothermobarometry of diamond inclusions from the Diavik mine, Slave craton (42 mW/m^2; Donnelly *et al.* 2007, Van Rythoven & Schulze 2009). Cooler geotherms were determined, however, for other occurrences of diamond on the Slave craton. Geothermobarometry of inclusions from the Panda mine yielded two apparent geothermal trends with corresponding surface heat-flows of 37 and 40–42 mW/m^2 (Stachel *et al.* 2003, Tappert *et al.* 2005). Snap Lake is slightly cooler with 40–41 mW/m^2 (Pokhilenko *et al.* 2004, Promprated *et al.* 2004). Inclusions in diamond crystals from the Kaapvaal craton give scattered results owing to re-equilibration of diamond inclusions because of temperature differences, but plot on cooler geotherms on average: 40 mW/m^2 (Phillips & Harris 1995, Stachel *et al.* 2003, Phillips *et al.* 2004).

Conclusions

The data from this suite of diamond crystals expand on the work of the few previous diamond-inclusion studies of this type on the Superior craton. Diamond from the Lynx kimberlite differs significantly from that at the nearby Renard kimberlite pipes (Hunt *et al.* 2008) in terms of physical characteristics and minerals included. The latter difference could be due to the very small sets of samples in both mineral-inclusion studies. The range of morphologies and resorption features for diamond from Lynx is typical of most primary diamond deposits, but there is a major abundance of brown tetrahexahedroida. This is in contrast to the diamond suite examined from nearby Renard, where colorless single crystals are an important component of the yield of commercial diamond (Fitzgerald *et al.* 2009).

There appears to be a possible correlation between light brown to brown stones with a P-type parentage, and colorless stones with an E-type parentage (based on a single crystal of diamond containing an E-type inclusion). The mineral inclusions indicate that at least three distinct parageneses can be assigned to the Lynx diamond crystals: harzburgitic, lherzolitic, and eclogitic. Geothermobarometric data suggest a relatively shallow lherzolitic zone in the diamond-stable Superior lithospheric mantle during the early Cambrian. The P–T conditions in the mantle during this time were consistent with a slightly elevated geothermal gradient relative to other diamond locales worldwide.

Acknowledgements

References

Birkett, T.C., McCandless, T.E. & Hood, C.T. (2003): Petrology of the Renard igneous bodies: host rock for diamonds in the northern Otish mountains region, Quebec. *8th Int. Kimberlite Conf.* (*Victoria*), *Extended Abstr.*

Bulanova, G.P., Griffin, W.L., Ryan, C.G., Shestakova, O.Ye. & Barnes, S.-J. (1996): Trace elements in sulfide inclusions from Yakutian diamonds. *Contrib. Mineral. Petrol.* **124**, 111-125.

Clifford, T.N. (1966): Tectono-metallogenic units and metallogenic provinces of Africa. *Earth Planet. Sci. Lett.* **1**, 421-434.

Craig, J.R. & Kullerud, G. (1969): Phase relations in the Cu–Fe–Ni–S system and their applications to magmatic ore deposits. *In* Magmatic Ore Deposits (H.D.B. Wilson, ed.). *Econ. Geol. Monogr.* **4**, 344-358.

Davies, R.M., Griffin, W.L., O'Reilly, S.Y. & Doyle, B.J. (2004): Mineral inclusions and geochemical characteristics of microdiamonds from the DO27, A154, A21, A418, DO18, DD17 and Ranch Lake kimberlites at Lac de Gras, Slave Craton, Canada. *Lithos* **77**, 39-55.

Davis, D.W. (2002): U–Pb geochronology of Archean metasedimentary rocks in the Pontiac and Abitibi subprovinces, Quebec, constraints on timing, provenance and regional tectonics. *Precamb. Res.* **115**, 97-117.

De Stefano, A., Lefebvre, N. & Kopylova, M. (2006): Enigmatic diamonds in Archean calc-alkaline lamprophyres of Wawa, southern Ontario, Canada. *Contrib. Mineral. Petrol.* **151**, 158-173.

Donnelly, C.L., Stachel, T., Creighton, S., Muehlenbachs, K. & Whiteford, S. (2007): Diamonds and their mineral inclusions from the A154 South pipe, Diavik diamond mine, Northwest Territories, Canada. *Lithos* **98**, 160-176.

Fisher, D. (2009): Brown diamonds and high pressure high temperature treatment. *Lithos* **112** (suppl. 2), 619-624.

Fitzgerald, C.E., Hetman, C.M., Lepine, I., Skelton, D.S. & McCandless, T.E. (2009): The internal geology and emplacement history of the Renard 2 kimberlite, Superior Province, Quebec, Canada. *Lithos* **112**, 513-528.

Grütter, H., Latti, D. & Menzies, A. (2006): Cr-saturation arrays in concentrate pyrope compositions from kimberlite and their use in mantle barometry. *J. Petrol.* **47**, 801-820.

GURNEY, J.J. (1984): A correlation between pyropes and diamonds in kimberlites. *In* Kimberlite Occurrence and Origin: a Basis for Conceptual Models in Exploration (J.E. Glover & P.G. Harris, eds.). *Geology Department and University Extension, University of Western Australia, Publ.* **8**, 143-166.

GURNEY, J.J., HARRIS, J.W. & RICKARD, R.S. (1984): Silicate and oxide inclusions in diamonds from the Orapa Mine, Botswana. *In* Kimberlites II: the Mantle and Crust–Mantle Relationships (J. Kornprobst, ed.). Elsevier, Amsterdam, The Netherlands (3-9).

GURNEY, J.J., HARRIS, J.W., RICKARD, R.S. & MOORE, R.O. (1985): Inclusions in Premier mine diamonds. *Trans. Geol. Soc. S. Afr.* **88**, 301-310.

HEAMAN, L.M., KJARSGAARD, B.A. & CREASER, R.A. (2004): The temporal evolution of North American kimberlites. *Lithos* **76**, 377-397.

HUNT, L., STACHEL, T. & MCCANDLESS, T. (2008): Diamonds from the Renard kimberlites, Quebec. *9th Int. Kimberlite Conf.* (*Frankfurt*), *Abstr.* **00185**.

KENNEDY, C.S. & KENNEDY, G.C. (1976): The equilibrium boundary between graphite and diamond. *J. Geophys. Res.* **81**, 2467-2470.

LEFEBVRE, N., KOPYLOVA, M. & KIVI, K. (2005): Archean calc-alkaline lamprophyres of Wawa, Ontario, Canada: unconventional diamondiferous volcaniclastic rocks. *Precamb. Res.* **138**, 57-87.

LEFEBVRE, N., KOPYLOVA, M., KIVI, K. & BARNETT, R.L. (2003): Diamondiferous volcaniclastic debris flows of Wawa, Ontario, Canada. *8th Int. Kimberlite Conf.* (Victoria), CD, not paginated.

MCCANDLESS, T.E., SCHULZE, D.J., BELLIS, A., TAYLOR, L.A., LIU, Y. & VAN RYTHOVEN, A.D. (2008): Morphology and chemistry of diamonds from the Lynx kimberlite dyke complex, northern Otish Mountains, Quebec. *9th Int. Kimberlite Conf.* (*Frankfurt*), *Abstr.* 00369.

MEYER, H.O.A. (1987): Inclusions in diamond. *In* Mantle Xenoliths (P.H. Nixon, ed.). John Wiley, Chichester, U.K. (501-522).

MEYER, H.O.A. & BOYD, F.R. (1972): Composition and origin of crystalline inclusions in natural diamonds. *Geochim. Cosmochim. Acta* **36**, 1255-1273.

NIMIS, P. & TAYLOR, W.R. (2000): Single clinopyroxene thermobarometry for pyrope peridotites. I. Calibration and testing of a Cr-in-Cpx barometer and an enstatite-in-Cpx thermometer. *Contrib. Mineral. Petrol.* **139**, 541-554.

NOYES, A.K., HEAMAN, L.M. & CREASER, R.A. (2011): A comparison of chronometers applied to Monastery kimberlite and the feasibility of U–Pb geochronology. *In* Dyke Swarms: Keys for Geodynamic Interpretation (R.K. Srivastava, ed.). Springer, Berlin, Germany (457-494).

PHILLIPS, D. & HARRIS, J.W. (1995): Geothermobarometry of diamond inclusions from the De Beers pool mines, Kimberley, South Africa. *Sixth Int. Kimberlite Conf.* (*Novosibirsk*), *Extended Abstr.*, 443.

PHILLIPS, D., HARRIS, J.W. & VILJOEN, K.S. (2004): Mineral chemistry and thermobarometry of inclusions from De Beers pool diamonds, Kimberley, South Africa. *Lithos* **77**, 155-179.

POKHILENKO, N.P., SOBOLEV, N.V., REUTSKY, V.N., HALL, A.E. & TAYLOR, L.A. (2004): Crystalline inclusions and C isotope ratios in diamonds from the Snap Lake/King Lake kimberlite dyke system: evidence of ultradeep and enriched lithospheric mantle. *Lithos* **77**, 57-67.

POLLACK, H.N. & CHAPMAN, D.S. (1977). On the regional variation of heat flow, geotherms, and lithospheric thickness. *Tectonophysics* **38**, 279-296.

PROMPRATED, P., TAYLOR, L.A., ANAND, M., FLOSS, C., SOBOLEV, N.V. & POKHILENKO, N.P. (2004): Multiple-mineral inclusions in diamonds from the Snap Lake/King Lake kimberlite dike, Slave craton, Canada: a trace-element perspective. *Lithos* **77**, 69-81.

ROBINSON, D.N., SCOTT, J.N., VAN NIEKERK, A. & ANDERSON, V.G. (1989): The sequence of events reflected in the diamonds of some southern African kimberlites. *In* Kimberlites and Related Rocks **2** (J. Ross *et al.*, eds.). *Geol. Soc. Aust., Spec. Publ.* **14**, 990-1000.

SCHULZE, D.J. (2003): A classification scheme for mantle-derived garnets in kimberlite: a tool for investigating the mantle and exploring for diamonds. *Lithos* **71**, 195-213.

SCULLY, K.R. (2000): *Mantle Xenoliths from the Attawapiskat Kimberlite Field, James Bay Lowlands, Ontario*. M.Sc. thesis, Department of Geology, University of Toronto, Toronto, Ontario.

SOBOLEV, N.V. (1977): *Deep-Seated Inclusions in Kimberlites and the Problem of the Composition of the Upper Mantle*. American Geophysical Union, Washington, D.C.

SOBOLEV, N.V., LOGVINOVA, A.M., ZEDGENIZOV, D.A., SERYOTKIN, Y.V., YEFIMOVA, E.S., FLOSS, C. & TAYLOR, L.A. (2004): Mineral inclusions in microdiamonds and macrodiamonds from kimberlites of Yakutia: a comparative study. *Lithos* **77**, 225-242.

SOBOLEV, N.V., POKHILENKO, N.P. & EFIMOVA, E.S. (1984): Diamond bearing peridotite xenoliths in kimberlites and the problem of the origin of diamonds. *Geologiya i Geofizika* **25**, 62-76 (in Russ.).

SOBOLEV, N.V., POKHILENKO, N.P., LAVREN'TEV, YU.G. & USOVA, L.V. (1978): The role of chromium in pyropes from kimberlites. *In* The Problems of Petrology of the Earth's Crust and the Upper Mantle. Nauka, Novosibirsk, USSR (145-168; in Russian).

SOBOLEV, N.V., YEFIMOVA, E.S. & KOPTIL, V.I. (1999): Mineral inclusions in diamonds in the Northeast of the Yakutian

diamondiferous province. *In* Proc. Seventh Int. Kimberlite Conf.; the P.H. Nixon volume (J.J. Gurney, J.L. Gurney, M.D. Pascoe & S.H. Richardson, eds.). Red Roof Design, Cape Town, South Africa (816-822).

STACHEL, T., BANAS, A., MUEHLENBACHS, K., KURZLAUKIS, S. & WALKER, E.C. (2006): Archean diamonds from Wawa (Canada): samples from deep cratonic roots predating the cratonization of the Superior Province. *Contrib. Mineral. Petrol.* **151**, 737-750.

STACHEL, T. & HARRIS, J.W. (2008): The origin of cratonic diamonds – constraints from mineral inclusions. *Ore Geol. Rev.* **34**, 5-32.

STACHEL, T., HARRIS, J.W., TAPPERT, R. & BREY, G.P. (2003): Peridotitic diamonds from the Slave and Kaapvaal cratons – similarities and differences based on a preliminary data set. *Lithos* **71**, 489- 503.

STACHEL, T., VILJOEN, K.S., MCDADE, P. & HARRIS, J.W. (2004): Diamondiferous lithospheric roots along the western margin of the Kalahari craton – the peridotitic inclusion suite in diamonds from Orapa and Jwaneng. *Contrib. Mineral. Petrol.* **147**, 32-47.

TAPPERT, R., STACHEL, T., HARRIS, J.W., SHIMIZU, N. & BREY, G.P. (2005): Mineral inclusions in diamonds from the Panda kimberlite, Slave Province, Canada. *Eur. J. Mineral.* **17**, 423-440.

TAYLOR, L.A. & LIU, Y. (2009): Sulfide inclusions in diamonds: not monosulfide solid solution. *Russ. Geol. Geophys.* **50**, 1201-1211.

TSAI, H.M., MEYER, H.O.A., MOREAU, J. & MILLEDGE, J. (1979): Mineral inclusions in diamond: Premier, Jagersfontein and Finsch kimberlites, South Africa, and Williamson mine, Tanzania. *In* Kimberlites, Diatremes, and Diamonds: their Geology, Petrology and Geochemistry (F.R. Boyd & H.O.A. Meyer, eds.). American Geophysical Union, Washington, D.C. (16-26).

VAN RYTHOVEN, A.D. & SCHULZE, D.J. (2009): In-situ analysis of diamonds and their inclusions from the Diavik mine, Northwest Territories, Canada: mapping diamond growth. *Lithos* **112**, 870-879.

VICKER, P. (1997): *Pyrope Peridotite Xenoliths from Kimberlite near Kirkland Lake, Canada.* M.Sc. thesis, University of Toronto, Toronto, Ontario.

VILJOEN, K.S., PHILLIPS, D., HARRIS, J.W. & ROBINSON, D.N. (1999): Mineral inclusions in diamonds from the Venetia kimberlites, Northern Province, South Africa. *In* Proc. Seventh Int. Kimberlite Conf.; the P.H. Nixon volume (J.J. Gurney, J.L. Gurney, M.D. Pascoe & S.H. Richardson, eds.). Red Roof Design, Cape Town, South Africa (888-895).

WEBB, K.J., SCOTT-SMITH, B.H., PAUL, J.L. & HETMAN, C.M. (2004): Geology of the Victor Kimberlite, Attawapiskat, northern Ontario, Canada: cross-cutting and nested craters. *Lithos* **76**, 29-50.

WILDING, M.C., HARTE, B. & HARRIS, J.W. (1991): Evidence for a deep origin for Saõ Luiz diamonds. *Proc. Fifth Int. Kimberlite Conf., Extended Abstr.* CPRM, Brasilia, Brazil (456-458).

YEFIMOVA, E.S., SOBOLEV, N.V. & POSPELOVA, L.N. (1983): Sulphide inclusions in diamond and specific features of their paragenesis. *Zap. Vses. Mineral. Obshshest.* **112**, 300-310 (in Russian).